Curvature of optimal control:
Deformation of scalar-input planar systems[*][†]

by

Matthias Kawski and Parnell Ted Maxwell

Department of Mathematics and Statistics
Arizona State University
Tempe, AZ 85287, USA

Abstract: The Pontryagin Maximum Principle and high-order open-mapping theorems generalize elementary first-derivative tests to nonlinear optimal control. They provide necessary conditions for a trajectory-control-pair to be optimal, or sufficient conditions for local controllability. Sufficient conditions for optimality (and necessary conditions for nonlinear controllability) are harder to obtain. Like the Legendre-Clebsch condition, they generally take the form of tests for definiteness of second order derivatives.

Recently, Agrachev introduced an attractive alternative by developing a notion of curvature of optimal control that generalizes classical Gauss (and Ricci) curvatures. This theory naturally applies to systems whose controls take values on a circle or sphere. In this article we present initial studies of how this notion of curvature provides insight into the limiting case when the circles become degenerate ellipses in the form of closed intervals. Of particular interest are well studied accessible, but uncontrollable, nonlinear systems, and systems that exhibit conjugate points, in which the control takes values in a closed interval $u = (u_1, u_2) \in [-1, 1] \times \{0\} \subseteq \mathbb{R}^2$. We focus on systems that are well-known models for the analysis of small-time local controllability and time-optimal control.

Keywords: optimal control, curvature.

1. Introduction

Consider the problem of deciding whether a trajectory pair (u^*, x^*): $[0, T] \mapsto U \times M^n$ of a generally nonlinear system $\dot{x} = F(x, u)$, $x \in M^n$, $u \in U \subseteq \mathbb{R}^m$, is a time-optimal solution connecting given endpoints $x(0) = x_0$ and $x(T) = x_T$ lying in an n-dimensional smooth manifold M^n, or whether the system is locally

controllable about this trajectory. The basic approach is to analyze whether the endpoint map $u \mapsto x(T; u)$ (for fixed T, and x_0) from a set of admissible controls $\mathcal{U}$ to $\mathbb{R}^n$, is locally an open map at the reference control $u^* \in \mathcal{U}$. A typical choice is $\mathcal{U} = L^1([0, T], U)$ with $U \subseteq \mathbb{R}^m$ convex and compact.

The primary tools are derivatives of this map that are based on control variations and that have desired convexity properties together with corresponding open mapping theorems, compare e. g. Bianchini and Kawski (2003), and Sussmann (2002, 2004) for selected recent innovations. Conditions such as the Pontryagin Maximum Principle and its improvements are basically sophisticated generalizations of the elementary first-derivative test for critical points. As such they generally provide necessary conditions for a reference control u^* to be an *extremal* (i. e., a critical point of the endpoint map). The contrapositives of such statements serve as sufficient conditions for nonlinear local controllability about the reference trajectory (x^*, u^*): if the derivative has full rank, then the end-point map is locally open at the reference trajectory, and the system is locally controllable about this trajectory.

Sufficient conditions for optimality (and, correspondingly, necessary conditions for nonlinear controllability) are considerably harder to obtain. Like the classical Legendre-Clebsch condition, these typically generalize tests for definiteness of second order derivatives. Other, more geometric arguments that extend the classical calculus of variations theory of *envelopes* to optimal control settings may be found in Sussmann (1986, 1989) and the references therein.

Recently, Agrachev introduced an attractive alternative by developing notions of curvature of optimal control that generalize classical Gauss and Ricci curvatures (see Agrachev and Sachkov, 2004, and Agrachev, Chtcherbakova, and Zelenko, 2005). These notions preserve a classical theorem of differential geometry which asserts that if the curvature is negative along an extremal, then the extremal is locally optimal. This captures the pictorial notion that in spaces of negative curvature geodesics move away from each other. In other words, distinct geodesics emanating from one point can intersect again only if the curvature is sufficiently positive along the curve segment. Thus, in principle, in order to conclude local optimality, one only needs to compute the curvature along an extremal and verify that it is nonnegative (or *"not too positive"*). In other words this approach yields sufficient conditions for (local) optimality.

While several general theoretical results utilizing this curvature have been forthcoming (see Agrachev, Chtcherbakova, and Zelenko, 2005, Agrachev, and Shcherbakova, 2005, and Serres, 2006), the size and complexity of the formulas for the curvature in local coordinates have so far severely limited explorations of this object for specific classes of systems. A significant complication of such calculations is due to the nature of the curvature being a (scalar) function on the circle-subbundle (or sphere-subbundle) of the cotangent bundle of the state-space. In other words, unlike Gaussian curvature which, in the two-dimensional case, is a scalar function on the state-space, this curvature of optimal control may at every point have different values in different directions.

The first notable explicit findings for specific classes of systems were obtained by Serres (2006) who studied *Zermelo's navigation problem*. In practical terms, this is the problem of finding time-optimal controls for a boat with steering control and with an engine providing relative unit speed but which is subject to a drift due to currents or wind. Formally consider systems in the plane of the form

$$
\begin{cases}
\dot{x}_1 &=& f_1(x_1, x_2) + u_1 \qquad\qquad \text{subject to} \\
\dot{x}_2 &=& f_2(x_1, x_2) + u_2 \qquad\qquad u_1^2 + u_2^2 = 1.
\end{cases}
\tag{1}
$$

One beautiful result of Serres (2006) is that if the matrix $(a_{ij}) \in \mathbb{R}^{2 \times 2}$ is self-adjoint, then extremals of the system with linear drift $f_i(x) = a_{i1}x_1 + a_{i2}x_2$ are locally optimal.

For the purpose of visualizing the curvature in this problem we developed interactive tools that require sizeable computations in the computer algebra system MAPLE and the numerical engine of MATLAB to obtain intriguing images that overlaid families of geodesics, geodesic spheres, and color-coded views of the curvature, selected static images are posted on-line (see Gehrig and Kawski, 2004). These tools allow one to experiment with various systems and nicely demonstrate the intricacy of the dependence of the curvature at any point in the state space on the direction in fibre, and its role in focusing geodesics. Indeed, one commonly observes multiple changes of sign in the curvature as the co-state rotates once about the zero-section.

Closely related work by Chitour and Sigalotti (2005) and Sigalotti and Chitour (2006), that in some sense is complementary, studies the "Dubins' car" on curved surfaces. This system is very similar to the boat, but instead of an external drift vector field (wind or current) and velocity controls (steering angle), the control is the rate of change of the steering angle. The drift term is due to the additional integration. In this case the curvature of the state space is the given starting point, and the authors investigate the structure of optimal trajectories.

After this general introduction, the subsequent sections review key definitions and aspects of Agrachev's curvature, and present an overview of the nature of the calculations when the control set is deformed from a circle to an interval via a family of ellipses.

2. Elements of Agrachev's theory of curvature of optimal control

This section reviews some elementary definitions, techniques, and results of Agrachev's theory. We follow closely the notation and language of Agrachev and Sachkov (2004). While more recent work by Agrachev, Chtcherbakova, and Zelenko (2005) extends the theory to higher dimensional settings, we here

restrict our attention to a special case of systems of the form (1) on a two dimensional state space.

Under mild regularity and convexity conditions, one may assume that (locally in x) the intersection $\mathcal{H}_x$ of the level set $\mathcal{H} = H^{-1}(1)$ of the maximized Hamiltonian H with each fibre $T_x^*\mathbb{R}^2$ is a simple closed convex curve that does not contain the origin. A key step is to compute a vertical vector field v on $T^*\mathbb{R}^2$ that satisfies the identity

$$L_v^2 s = -s + bL_v s \tag{2}$$

where $s = p_1 dx_1 + p_2 dx_2$ is the tautological one-form on $T^*\mathbb{R}^2$ restricted to $\mathcal{H}$, and L_v denotes the Lie derivative in the direction of the vector field v. The key requirement is the (negative) unit coefficient of the first term on the right hand side of (2). This identity uniquely determines a vector field v up to multiplication by -1.

The vector field v may be computed explicitly as follows. Start by introducing polar coordinates $(p_1, p_2) = (r\cos\varphi, r\sin\varphi)$ on the fibres of $T^*\mathbb{R}^2$. With these, the level sets $\mathcal{H}_x$ are parameterized by the angle φ (using that $\mathcal{H}_x$ does not pass through the origin and that it is convex), and we write $p = p(\varphi)$. Differentiating twice, and using the linear independence of p and p', decompose the second derivative with respect to φ as a linear combination

$$p''(\varphi) = a_1(\varphi)p(\varphi) + a_2(\varphi)p'(\varphi). \tag{3}$$

Next perform a change of parameters $\theta = \theta(\varphi)$ so that

$$a_1(\varphi) \cdot \left(\frac{d\theta}{d\varphi}\right)^2 = -1. \tag{4}$$

Up to translation and orientation this condition uniquely determines the new parameter θ, which, abusing notation, is such that

$$p''(\theta) = -p(\theta) + a_2(\theta)p'(\theta). \tag{5}$$

Consequently, with either choice of sign, $v = \frac{\partial}{\partial\theta} = \frac{\pm 1}{\sqrt{-a_1}}\frac{\partial}{\partial\varphi}$ is the desired vertical field. Next combine this field with the Hamiltonian field $\vec{h}$ and their Lie bracket to obtain a moving frame

$$V_1 = v, \quad V_2 = [v, \vec{h}], \quad V_3 = \vec{h} \tag{6}$$

on the level surface $H^{-1}(1) \subseteq T^*\mathbb{R}^2$. It is straightforward to verify their independence at all points on $\mathcal{H}$. One also readily verifies that the Lie derivatives of the fields in this frame in the direction of the Hamiltonian vector field $\vec{h}$ satisfy

$$[\vec{h}, V_1] = -V_2, \quad [\vec{h}, V_2] = \kappa V_1, \quad [\vec{h}, V_3] = 0 \tag{7}$$

where κ is a scalar function on $\mathcal{H}$ and is called the curvature of the control system (1). This frame is particularly convenient for writing the Jacobi equation along an extremal (x_t, p_t) on $\mathcal{H}$. More specifically, in this moving frame the matrix

representation $\Gamma(t)$ of the operator $e^{t\,\mathrm{ad}\,\vec{h}}$ satisfies the linear differential equation

$$\dot{\Gamma}(t) = \Gamma(t) \cdot A(t) \tag{8}$$

with initial condition $\Gamma(0) = I_{3\times 3}$ where the coefficient matrix is given by

$$A(t) = \begin{pmatrix} 0 & \kappa(x_t, p_t) & 0 \\ -1 & 0 & 0 \\ 0 & 0 & 0 \end{pmatrix} . \tag{9}$$

A time $t_c > 0$ is, by definition, a conjugate time for an extremal (x_t, p_t) if the intersection of the vertical subspace $\Pi_0 = T_{p_0}(T_{x_0}^* \mathbb{R}^2)$ with its image $B_{t_c}\Pi_0$ under the flow B_t defined by the Jacobi equation is strictly larger than the subspace of constant solutions of the Jacobi equation. Such an instant t_c corresponds to a nontrivial solution of the scalar boundary value problem

$$\ddot{y} + \kappa_t y = 0, \ \ y(0) = y(t_c) = 0. \tag{10}$$

It is clear from elementary differential equations that nontrivial solutions do not exist when $\kappa \leq 0$ for all times along an extremal (x_t, p_t). Moreover, in the case of not necessarily negative curvature, standard integral estimates yield lower bounds on the first positive conjugate time t_c.

Summarizing, in order to apply this sufficiency criterion for local optimality, i. e., for the absence of conjugate points, the main steps in the calculation are

- find the change of parameters $\theta = \theta(\varphi)$ so that (4) holds,
- calculate the curvature from $[\vec{h}, [\vec{h}, v]] = -\kappa v$, and
- verify that $\kappa \leq 0$ along an extremal, or find bounds for the integral of κ along the extremal if $\kappa \geq 0$ for some t.

As simple as these foregoing calculations appear, they quickly lead to large formulas, even for very simple system data f_1 and f_2. The case of a linear field $f_1\frac{\partial}{\partial x_1} + f_2\frac{\partial}{\partial x_2} = (a_{11}x_1 + a_{12}x_2)\frac{\partial}{\partial x_1} + (a_{21}x_1 + a_{22}x_2)\frac{\partial}{\partial x_2}$ with constant $a_{ij} \in \mathbb{R}$ was analyzed in detail by Serres (2006), while our simulations and visualization efforts concentrated on quadratic and globally bounded fields such as e. g. $(f_1, f_2) = (0, \mathrm{sech}\, x)$ (Gehrig and Kawski, 2004). Aside from the expected appearance of various products of derivatives of the drift (f_1, f_2), impressive is the complicated nature of the combination of higher harmonics $\cos j\theta$ and $\sin j\theta$ for $j = 1, 2, 3, 4$ in the formulas for the curvature κ which routinely allows the curvature at one point in the base to change sign a large number of times as the direction varies.

3. Deformations of the control set

The main focus of this article is the investigation of how curvature and conjugate points change when the set of controlled velocities $\{(u_1, \varepsilon u_2): u_1^2 + u_2^2 = 1\}$ is continuously deformed into the interval $I = [-1, 1]$. For computational convenience we implement this by adding the parameter ε into the controlled vector

field as follows, leaving the set of control values $U = S^1$ the same, and consider systems of the form

$$\begin{cases} \dot{x}_1 & = & f_1(x_1, x_2) + u_1 \qquad \text{subject to} \\ \dot{x}_2 & = & f_2(x_1, x_2) + \varepsilon u_2 \qquad u_1^2 + u_2^2 = 1. \end{cases} \qquad (11)$$

Of particular interest are deformations of the systems

$$\begin{cases} \dot{x}_1 & = & u_1 \\ \dot{x}_2 & = & x_1^m + \varepsilon u_2 \end{cases} \qquad (12)$$

and

$$\begin{cases} \dot{x}_1 & = & -x_2 + u_1 \\ \dot{x}_2 & = & x_1 + \varepsilon u_2 \end{cases} \qquad (13)$$

which are well understood in the limiting single-input case of $\varepsilon = 0$. We are interested in how their properties arise as limits of deformations of the corresponding systems of the form (11). The first family of systems is small-time locally controllable if and only if m is odd. If m is even, the reachable sets exhibit well-known *fold-overs* (see Hermes, 1967) with consequent appearance of conjugate points (compare Sussmann, 1989). The second system is the controlled harmonic oscillator whose switching curves consisting of two infinite families of semicircles are standard examples in textbooks on optimal control.

Due to the continuity of the map from controls $u(\cdot) \in \mathcal{U} \subseteq L^1([0, T], S^1)$ to trajectories $x(\cdot; u) \in C([0, T], \mathbb{R}^2)$, it is clear that as ε varies from 1 to 0 the corresponding trajectories vary continuously. Given the absence of nontrivial singular extremals in the systems (12) and (13), the bang-bang extremals of these systems are approximated by continuously (in time) varying optimal controls. One expects, and this is confirmed in simulations, that these optimal controls change from comparatively slowly varying to rapid transitions as ε decreases from one to near zero. Fig. 1 shows the typical evolution of the co-state in polar coordinates. In this figure, the angle φ is not yet the geometric object θ identified in the curvature formula, yet the curves still nicely exhibit the qualitative evolution of the direction of the co-state.

This work was motivated by the possibility of using the well-defined curvature for determining conjugate points and optimal extremals for systems with small-values of $\varepsilon > 0$, and by passing to the limit to conclude respective properties of the limiting systems whose control sets are compact intervals. Relying on suitable continuity and structural stability arguments, this can be justified rigorously under suitable hypotheses (e. g. isolated switching times). For a detailed discussion of conjugate points for bang-bang extremals for systems whose control set is a line-segment, or more generally, a cube (see Schättler, 1990, and Sussmann, 1986). Evidently, without further technical hypotheses one cannot conclude that the existence or non-existence of conjugate points is preserved by
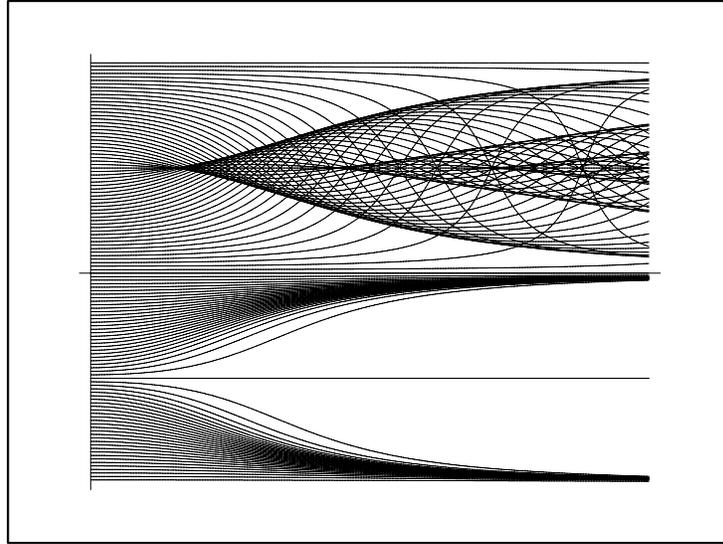
Figure 1. Time evolution of angle φ for (12) with $m = 2$, $\varepsilon = 0.2$, $T = 3.5$.

the limit as $\varepsilon \longrightarrow 0$. However, for specific systems of interest such conclusions may be warranted. In this particular work the main thrust is not the general abstract theorem, but to actually test the computational feasibility of this approach by analyzing deformations of specific systems, in particular deformations of the well-understood ones listed above, and explore what information can be extracted from these. In some sense the main result is a negative one as the size of the ensuing formulas for the curvature of the deformed systems far exceeds all expectations. This observation leads one to conclude that for typical systems similar to those of form (12) or (13) (with more complicated right hand sides) this approach via deformations might not be practical as compared to a direct analysis of the limiting system. This, of course, does not rule out conclusions about the properties of the limiting system obtained from general properties of the deformed systems.

Nonetheless, the curvature calculations are feasible with the use of a computer algebra system, and aside from using these to visualize the interplay of curvature, extremal trajectories, and geodesic spheres (see Gehrig and Kawski, 2004), these also were the basis for numerical simulation of the rotation of the vertical field along extremal trajectories, compare Fig. 2. Due to inherent limitations of this hard-copy special issue article, we will in the sequel only summarize the initial calculations which suggest the resulting size of the formulas for the curvature (but also their expected manageability using computer algebra) and provide still-images taken from the computed animations. Samples of both the
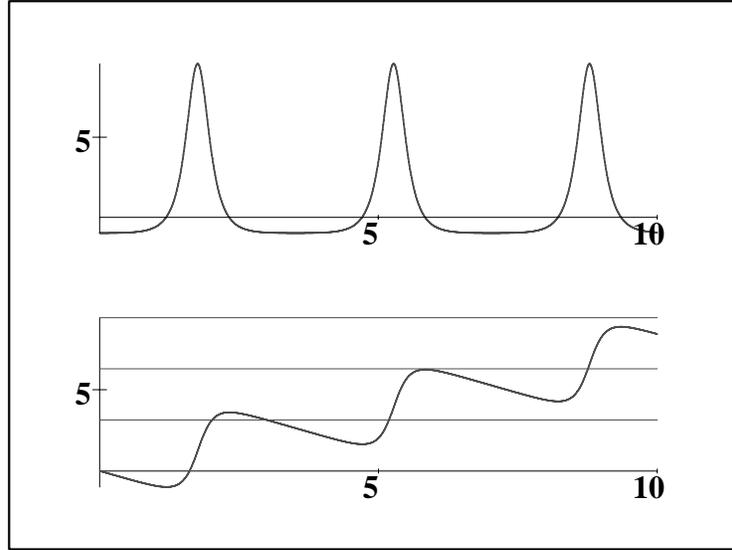
Figure 2. The curvature and its primitive as functions of time along extremal of system (12) with $m = 2$, $\varepsilon = 1$, $p(0) = (0.94, \sqrt{0.34})$

full computations and live animations of the deformations of the structures of extremal trajectories will be made available online at the first author's WWW-site.

We begin our calculations for the general system (11), and specialize later to the deformed power integrator (12) and the deformed controlled harmonic oscillator (13). Following the general approach outlined in Section 2, we form the Hamiltonian and compute the maximizing controls. We suppress dependencies such as $f_1(x_1, x_2)$ and simply write f_1 etc. when it will not cause confusion. The control dependent Hamiltonian H_u is

$$H_u(x, p) = p_1(u_1 + f_1) + p_2(\varepsilon u_2 + f_2). \tag{14}$$

Subject to the constraint $u_1^2 + u_2^2 = 1$, at each point $(x, p) \in T^*\mathbb{R}^2$ with $p \neq 0$ this control dependent Hamiltonian H_u is maximized by the uniquely determined control values

$$u_1^* = \frac{p_1}{\sqrt{p_1^2 + \varepsilon^2 p_2^2}} \quad \text{and} \quad u_2^* = \frac{\varepsilon p_2}{\sqrt{p_1^2 + \varepsilon^2 p_2^2}}. \tag{15}$$

Upon introduction of polar coordinates $(p_1, p_2) = (r \cos\varphi, r \sin\varphi)$ in the fibres, the maximized Hamiltonian becomes:

$$H^*(x, r \cos\varphi, r \sin\varphi) = f_1 r \cos\varphi + f_2 r \sin\varphi + r \sqrt{\cos^2\varphi + \varepsilon^2 \sin^2\varphi}. \tag{16}$$

Note that in the special case of $\varepsilon = 1$ (no deformation, studied in detail in e. g. Serres, 2006) the last term is constant equal to one, which much simplifies all subsequent calculations.

In the general case of $\varepsilon \in [0, 1]$ the Hamiltonian vector field in polar coordinates is

$$
\begin{aligned}
\vec{h} \;=\; & \left(f_1 + \frac{\cos\varphi}{\sqrt{\cos^2\varphi + \varepsilon^2 \sin^2\varphi}} \right) \frac{\partial}{\partial x_1} \\
& + \left(f_2 + \frac{\varepsilon^2 \sin\varphi}{\sqrt{\cos^2\varphi + \varepsilon^2 \sin^2\varphi}} \right) \frac{\partial}{\partial x_2} \\
& - \left(\cos^2\varphi \frac{\partial f_1}{\partial x_1} + \sin^2\varphi \frac{\partial f_2}{\partial x_2} + \cos\varphi \sin\varphi \left(\frac{\partial f_2}{\partial x_1} + \frac{\partial f_1}{\partial x_2} \right) \right) r \frac{\partial}{\partial r} \\
& + \left(\sin^2\varphi \frac{\partial f_2}{\partial x_1} - \cos^2\varphi \frac{\partial f_1}{\partial x_2} + \cos\varphi \sin\varphi \left(\frac{\partial f_1}{\partial x_1} - \frac{\partial f_2}{\partial x_2} \right) \right) \frac{\partial}{\partial \varphi}.
\end{aligned}
$$

Note that there is some redundancy in this formula as the Hamiltonian vector field is tangent to the three dimensional level surfaces of the Hamiltonian, and one could express the radial component as a function of the angle φ. However, in the formula stated here, the direction $\frac{\partial}{\partial \varphi}$ is interpreted in terms of polar coordinates on the entire fibre $T_x \mathbb{R}^2$. This format is convenient for subsequent calculations of the double Lie bracket for the curvature using a computer algebra system.

Not to be confused with the above, also use the *angle* φ to parameterize the intersection of the level sets $H^{-1}(1)$ of the Hamiltonian with the fibres. (Of course, to this corresponds a different meaning of the symbol $\frac{\partial}{\partial \varphi}$.) To avoid possible misinterpretations, write this curve as $p(\varphi) = (\varrho(\varphi) \cos\varphi, \varrho(\varphi) \sin\varphi)$. From the equation $H(x, \varrho(\varphi) \cos\varphi, \varrho(\varphi) \sin\varphi) \equiv 1$ one obtains the explicit formula

$$
\varrho(\varphi) = \frac{1}{f_1 \cos\varphi + f_2 \sin\varphi + \sqrt{\cos^2\varphi + \varepsilon^2 \sin^2\varphi}} \,. \tag{17}
$$

To determine the change of parameters to the distinguished angular variable θ, calculate the coefficient $a_1 = -\left(\frac{d\varphi}{d\theta} \right)^2$ in the linear combination of the second derivative $p''(\varphi) = a_1 p(\varphi) + a_2 p'(\varphi)$. A simple calculation yields

$$
a_1 = \frac{\varrho''}{\varrho} - 2 \left(\frac{\varrho'}{\varrho} \right)^2 - 1. \tag{18}
$$

In the previously studied undeformed case $\varepsilon = 1$ the square root evaluates to one, much simplifying all subsequent work, and from

$$
\begin{aligned}
\varrho' \;&=\; \varrho^2 (f_1 \sin\varphi - f_2 \cos\varphi) & (19) \\
\varrho'' \;&=\; 2\varrho \varrho' (f_1 \sin\varphi - f_2 \cos\varphi) + \varrho^2 (f_1 \cos\varphi + f_2 \sin\varphi) & (20)
\end{aligned}
$$

straightforward simplifications yield $a_1 = -\varrho$. Hence in the undeformed case $\varepsilon = 1$, from the condition $a_1 \left(\frac{d\theta}{d\varphi}\right)^2 = -1$, the desired vertical vector field is

$$v = \frac{\partial}{\partial \theta} = \frac{1}{\sqrt{1 + f_1 \cos \varphi + f_2 \sin \varphi}} \frac{\partial}{\partial \varphi}. \tag{21}$$

In the general case with deformations $0 < \varepsilon < 1$ analogous calculations are readily performed using a computer algebra system, and the details of the intermediate formulas are of little interest by themselves. After simplifications one obtains

$$\frac{\partial}{\partial \theta} = \frac{\varepsilon}{\sqrt{\Delta^3 (\Delta + f_1 \cos \varphi + f_2 \sin \varphi)}} \cdot \frac{\partial}{\partial \varphi} \tag{22}$$

where $\Delta = \sqrt{\cos^2 \varphi + \varepsilon^2 \sin^2 \varphi}$.

The next step in the calculation is to compute the curvature κ from some component of the double bracket identity

$$[\vec{h}, [\vec{h}, v]] = -\kappa v. \tag{23}$$

In the undeformed case $\varepsilon = 1$ this is a cumbersome calculation by hand but quite straightforward using a recent version of a computer algebra system. We note that just a few years ago, MAPLE release 8 could not simplify the resulting rational expression in the components f_1, f_2, their first two partial derivatives, and trigonometric terms involving $\cos j\varphi$ and $\sin j\varphi$ with j taking values from 0 to 4. Newer releases, relying especially on improved Gróbner bases tools reduce the quotient of originally 782 terms and 23 terms in numerator and denominator, respectively, to the polynomial expression that was given by Serres (2006). For particular systems such as the undeformed systems (12) and (13) in the case of $\varepsilon = 1$ these reduce much further to expressions that are amenable to detailed analysis.

However, for the general parameter-dependent case of $0 < \varepsilon < 1$ even the newest release 12 of MAPLE does not yield simplifications that provide much structural insight, nor are suitable for reproduction here. Nonetheless, the expressions are still useful for qualitative studies and for simulations of, e. g., the evolution (rotation) of the 3-frame on the surface $H^{-1}(1)$, i. e., in the time-varying second order differential equation (10). Compare Fig. 1 for a closely related plot of the time evolution of the *angle* of the co-state for system (12) with $m = 2$ due to the curvature. The plots of the special variable θ along extremals are qualitatively similar, compare Fig. 2.

We now concentrate on specific systems, and present selected formulas and graphical results of some simulations. First consider deformations of the uncontrollable quadratic planar system

$$\Sigma_\varepsilon : \begin{cases} \dot{x}_1 &= u_1 \\ \dot{x}_2 &= x_1^2 + \varepsilon u_2 \ . \end{cases} \tag{24}$$

In this case, the Hamiltonian and distinguished vertical vector fields reduce to

$$\vec{h} \;=\; \frac{\cos\varphi}{\sqrt{\cos\varphi^2 + \varepsilon^2 \sin^2\varphi}} \cdot \frac{\partial}{\partial x_1} \tag{25}$$

$$+ \left(x_1^2 + \varepsilon \cdot \frac{\varepsilon \sin\varphi}{\sqrt{\cos\varphi^2 + \varepsilon^2 \sin^2\varphi}} \right) \cdot \frac{\partial}{\partial x_2}$$

$$- x_1 r \sin 2\varphi \cdot \frac{\partial}{\partial r} \quad - \quad x_1 (1 - \cos 2\varphi) \cdot \frac{\partial}{\partial \varphi}$$

and

$$\frac{\partial}{\partial\theta} = \frac{\varepsilon}{\sqrt{\Delta^3(\Delta + x^2 \sin\varphi)}} \cdot \frac{\partial}{\partial\varphi} \quad \text{where,} \quad \Delta = \sqrt{\cos^2\varphi + \varepsilon^2 \sin^2\varphi}. \tag{26}$$

For the iterated Lie brackets and for the curvature κ we have not been able to achieve significant simplifications, and the formulas remain basically only amenable to numerical studies, very unlike the case of $\varepsilon = 1$ which allows analytic approaches, ruling out the existence of conjugate points or finding lower bounds for the time of the first conjugate point. In that special case of no deformation $\varepsilon = 1$, the curvature is given by the simple formula

$$\kappa \;=\; -\tfrac{9}{4} \sin(\varphi) - \tfrac{1}{4} \sin(3\varphi) - x_1^2 \big(\tfrac{21}{8} - 3\cos(2\varphi) + \tfrac{3}{8}\cos(4\varphi)\big). \tag{27}$$

Fig. 2 provides a typical picture for the curvature and its integral as functions of time along an extremal, showing the times when the image $B_{t_c}\Pi_0$ of the distinguished vertical subspace $\Pi_0 = T_{p_0}(T^*_{x_0}\mathbb{R}^2)$ has rotated by π, yielding a nontrivial intersection and thus a conjugate point. Numerical simulations indicate that as $\varepsilon \longrightarrow 0$, as expected, the peaks of $\kappa(t)$ become narrower and sharper, and correspondingly its primitive converging pointwise to a piecewise continuous function (compare Agrachev and Sachkov, 2004).

The corresponding typical portraits of families of projections of extremals into the state-space and the geodesic spheres are presented in Figs. 3 and 4. For small final times T and $\varepsilon \approx 1$, the reachable sets are almost perfect spheres. As time T increases, or the deformation parameter ε decreases, the reachable sets and structure of the extremals approach the familiar image of the reachable set of system (24) that is characterized by a sequence of *fold-overs* and corresponding emergence of conjugate points beyond which the extremals are no longer optimal (compare Hermes, 1967).

Fig. 3 illustrates the effect of the drift for larger times which breaks the symmetry of the perfect sphere of the driftless case. Fig. 4 illustrates the emergence of the first fold-overs.

Note that systems of form (12) possess symmetries in the form of homogeneity with respect to families of dilations. Consequently, the reachable sets reflect these symmetry properties for corresponding times and deformations. More specifically, one may fix a time T and vary only the deformation parameter ε, or vice versa. Except for the limiting case of $\varepsilon = 0$ and rescaling of the state-space, the corresponding reachable sets and families of extremals will exhibit the same
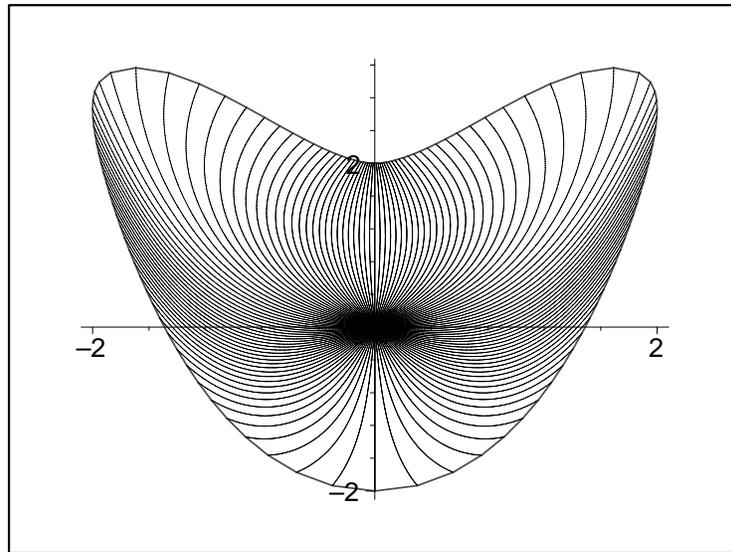
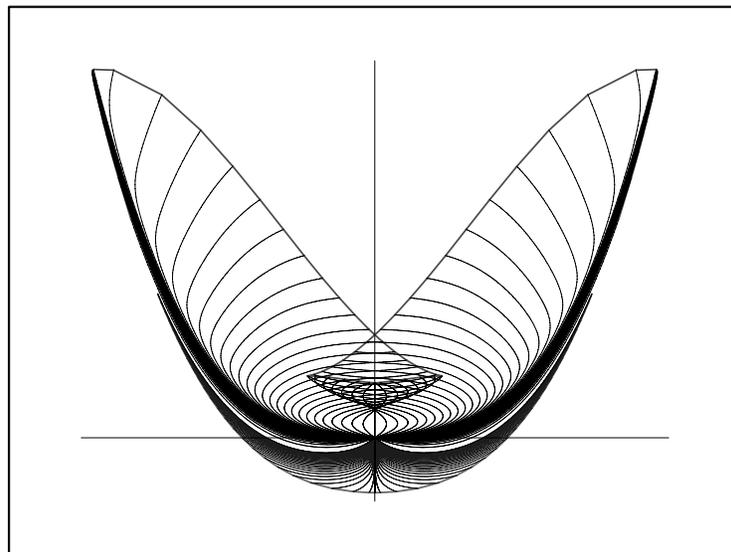Figure 3. Reachable set at $T = 2$ of system (12) with $m = 2$, $\varepsilon = 1$

Figure 4. Reachable set at $T = 2$ of system (12) with $m = 2$, $\varepsilon = 0.2$

qualitative properties. The choice of pairs (T, ε) such as in Fig. 1 is thus mainly guided by aesthetic reasons, with main focus on an aspect ratio that is suitable for observing the structural properties such as folds and conjugate points.

Specifically, in the case of exponent $m = 2$ in system (12) define the rescaling and families of dilations

$$\Delta_\delta(x_1, x_2) \quad = \quad (\delta x_1, \delta^2 x_2), \text{ and} \tag{28}$$

$$(u_1, u_2)^{\delta,\varepsilon}(t) \quad = \quad (\delta u_1(\delta t), \varepsilon \delta u_2(\delta t)). \tag{29}$$

One easily verifies that the corresponding trajectories $x^\varepsilon(\cdot\,;u)$ of system Σ^ε in (24) satisfy

$$x^1(\delta T; u^{\delta,\varepsilon}) = \Delta_\delta(x^\varepsilon(T;u)). \tag{30}$$
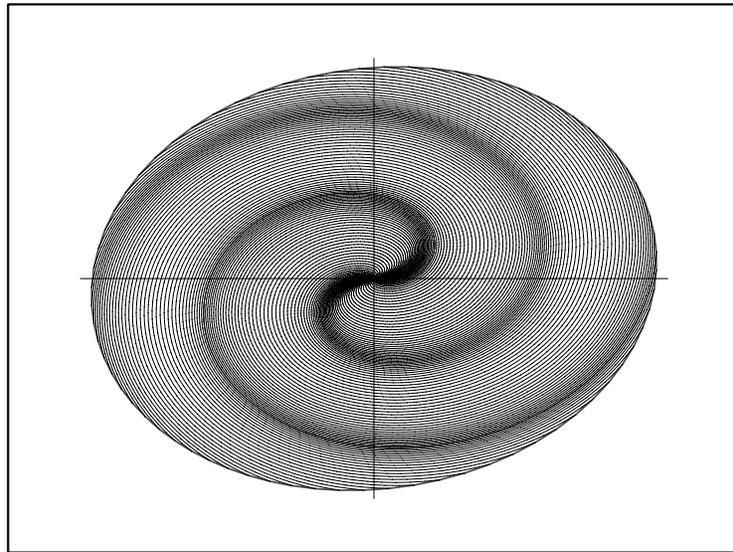

Figure 5. Reachable set at $T = \frac{5}{2}\pi$ of system (13) with $\varepsilon = 0.5$

For the deformed, controlled harmonic oscillator (13) there are no conjugate points for any value of $\varepsilon \in (0, 1]$. For $\varepsilon = 1$ all extremals remain uniformly spaced with co-state uniformly rotating around the circle. For $\varepsilon = 0$ one has the familiar picture of switching surfaces made up of families of semi-circles. For values of $0 < \varepsilon < 1$ one can nicely observe the emergence of zones of more densely packed extremals which uniformly converge to the well-known switching curves as $\varepsilon \longrightarrow 0$, compare Fig. 5.

4. Summary and conclusion

We initiated the study of how the theory of curvature of optimal control, which was originally formulated for control sets that are spheres, may be used to gain insight into the structure of optimal controls, and, in particular, absence

or presence of conjugate points for systems whose controls take values in an interval. The approach implements a classical method of *fattening* the line segment of admissible controls and continuously deforming it into a family of ellipses. While the size of the formulas obtained was beyond any expectations, and so far precludes analytic investigation in the general case, the formulas nonetheless are suitable for numerical simulations and qualitative studies that confirm expectations.

Acknowledgments

References

AGRACHEV, A., CHTCHERBAKOVA, N., and ZELENKO, I. (2005) On curvatures and focal points of dynamical Lagrangian distributions and their reductions by first integrals. *J. Dynamical and Control Systems* **11**, 297–327.

AGRACHEV, A. and SACHKOV, YU. (2004) *Control Theory from the Geometric Viewpoint.* Springer, Berlin.

AGRACHEV, A. and SHCHERBAKOVA, N. (2005) Hyperbolicity of Hamiltonian systems of negative curvature. *Dokl. Akad. Nauk* **400**, 295–298.

BIANCHINI, R., and KAWSKI, M. (2003) Needle variations that cannot be summed. *SIAM J. Control Optim.* **42**, 218–238.

CHITOUR, Y. and SIGALOTTI, M. (2005) On the controllability of the Dubins problem for surfaces. *J. Geom. Anal.* **15**, 565-587.

GEHRIG, E. and KAWSKI, M. (2004) Visualizing the curvature of optimal control. `http: // math. asu. edu/ ~kawski/ MATLAB/ control/ curvature. html`.

HERMES, H. (1967) Attainable sets and generalized. geodesic spheres. *J. Diff. Eqs.* **3**, 256–270.

SCHÄTTLER, H. (1990) Regularity properties of optimal trajectories: Recently developed techniques. *Monogr. Textbooks Pure Appl. Math.* **133**, 351–381,

SERRES, U. (2006) The curvature of 2-dimensional optimal control systems and Zermelo's navigation problem. *J. Math. Sciences* **135**, 3224–3243.

SIGALOTTI, M. AND CHITOUR, Y. (2006) Dubins' problem on surfaces. II. Nonpositive curvature. *SIAM J. Control Optim.* **45**, 457-482.

SUSSMANN, H. (1986) Envelopes, conjugate points and optimal bang-bang extremals. *Math. Appl.* **29**, 325–346.

SUSSMANN, H. (1989) Envelopes, high-order optimality conditions and Lie brackets. *Proc.* 28th *IEEE Conf. Decision Control*, 1107–1112.

SUSSMANN, H. (2002) High-order open mapping theorems. *Lect. Notes Control Inform. Sci.* **286**, 293–316.

SUSSMANN, H. (2004) Generalized differentials, variational generators, and the maximum principle with state constraints. *Lect. Notes Math.* **1932**, 221–284.